

# Mantle transition zone variations beneath the Ethiopian Rift and Afar: Chemical heterogeneity within a hot mantle?

D. G. Cornwell,<sup>1</sup> G. Hetényi,<sup>2</sup> and T. D. Blanchard<sup>1</sup>

Received 4 April 2011; revised 7 July 2011; accepted 9 July 2011; published 23 August 2011.

[1] The mantle transition zone (MTZ) structure beneath the Ethiopian Rift and Afar is mapped using receiver functions. The 410 discontinuity is flat and regionally depressed by 30–40 km, most likely due to a hot ( $\geq +250$  °C) and slow (average  $\delta V_S > 3$  %) upper mantle. The 660 discontinuity is shown to have variations in depth (665–705 km) over short length scales (<200 km). This results in a MTZ with a ‘normal’ average thickness of 244 km, (i.e., within error of the observed global average). However, local thickness variations (<230 km to >260 km) indicate possible compositional/chemical heterogeneities and elevated ambient temperatures near the base of the MTZ. These observations provide evidence for a link between the low velocity anomalies of the Ethiopian upper mantle and the African Superplume in the lower mantle. **Citation:** Cornwell, D. G., G. Hetényi, and T. D. Blanchard (2011), Mantle transition zone variations beneath the Ethiopian Rift and Afar: Chemical heterogeneity within a hot mantle?, *Geophys. Res. Lett.*, 38, L16308, doi:10.1029/2011GL047575.

## 1. Introduction

[2] East Africa is underlain by one of the most striking features of the lower mantle: the African Superplume [e.g., Ritsema *et al.*, 1999]. Numerous regional seismological studies [e.g., Benoit *et al.*, 2006; Bastow *et al.*, 2008; Chang and Van der Lee, 2011] favor the hypothesis that this broad (>500 km-wide) low velocity body extends across the mantle transition zone (MTZ) somewhere in the region of Kenya/Ethiopia but limited depth resolution usually renders this claim uncertain. Also unclear is the extent to which the low velocity zone beneath Ethiopia is a purely thermal anomaly, or one in which chemical heterogeneity also plays an important role. To address these issues we perform here a receiver function study of the Ethiopian MTZ.

[3] Mean global MTZ thickness has been measured at  $242 \pm 2$  km [Lawrence and Shearer, 2006] or 247 km [Tauzin *et al.*, 2008], although the actual depth of the seismic discontinuities at approximately 410 (the ‘410’) and 660 km (the ‘660’) is controlled by local temperature and composition of the mantle [e.g., Deuss, 2007]. If hot plumes pass through the MTZ, they are commonly predicted to cause an overall thinning by deepening the mineral phase transition of olivine ( $\alpha$ ) to wadsleyite ( $\beta$ -olivine) from 410 km depth and shallowing the mineral phase transition of ringwoodite to Mg-perovskite + magnesiowustite from 660 km depth [e.g.,

Helffrich, 2000], assuming that olivine dominates the mantle composition. Recent studies, however, suggest that another phase transition involving garnet (majorite  $\rightarrow$  Ca-perovskite) also takes place near 660 km depth or below, particularly if mantle potential temperatures are elevated [e.g., Vacher *et al.*, 1998]. The proportion of olivine-dominated (pyrolite [Ringwood, 1975]) and garnet-dominated (piclogite [Anderson and Bass, 1986]) mantle compositions is not ubiquitous and may change from one region to another.

[4] Previous MTZ thickness studies beneath Ethiopia/Afar either illuminated the MTZ beneath permanent seismological stations [e.g., Nyblade *et al.*, 2000; Tauzin *et al.*, 2008] or did not successfully image both the ‘410’ and ‘660’ beneath the region [Benoit *et al.*, 2006] and therefore do not place constraints on the lateral changes in MTZ thickness that are required to assess whether the African Superplume intersects the MTZ beneath Ethiopia.

[5] We use seismological data from stations in Ethiopia to identify the MTZ and map changes in its thickness beneath the Ethiopian rift, Afar and the uplifted Ethiopian Plateau. The receiver function (RF) method with subsequent migration using a regional velocity model produces a MTZ thickness map. We aim to test if a hot thermal anomaly has affected the MTZ beneath Ethiopia whilst considering the effects of lateral variations in composition and temperature.

## 2. Geodynamic Setting

[6] Hotspot tectonism in Ethiopia (Figure 1), which is characterised by Cenozoic continental flood basalt volcanism, plateau uplift and a transition from continental rifting to incipient seafloor spreading [Ebinger and Casey, 2001], is probably the result of a thermal plume that may extend from the Core–Mantle Boundary (CMB) [e.g., Simmons *et al.*, 2007]. The triple junction that links the Main Ethiopian rift (MER), Red Sea and Gulf of Aden is located within the Afar Depression and is believed to have started rifting during the Miocene [e.g., Wolfenden *et al.*, 2004]. The Afar Depression and MER are still magmatically active [e.g., Wright *et al.*, 2006]. Geophysical measurements in the Ethiopia–Afar region imaged a thinned crust and lithosphere beneath rifted areas compared to the uplifted Ethiopian Plateau [e.g., Dugda *et al.*, 2007; Cornwell *et al.*, 2010].

[7] In the mantle, RF studies using permanent stations show a normal MTZ thickness ( $\sim 250$  km at both FURI and ATD [Tauzin *et al.*, 2008];  $244 \pm 19$  and  $250 \pm 16$  km respectively at ATD and AAE [Nyblade *et al.*, 2000]), suggesting that a broad thermal anomaly beneath Afar does not extend to the MTZ. Tauzin *et al.* [2008] observed both discontinuities to be depressed by 30–50 km, most likely caused by the use of a velocity model without slow upper mantle anomalies. A study using regional deployments [Benoit *et al.*, 2006] found the MTZ beneath Ethiopia to be complex and

<sup>1</sup>School of Earth and Environment, University of Leeds, Leeds, UK.

<sup>2</sup>Institut für Geochemie und Petrologie, ETH Zurich, Zurich, Switzerland.

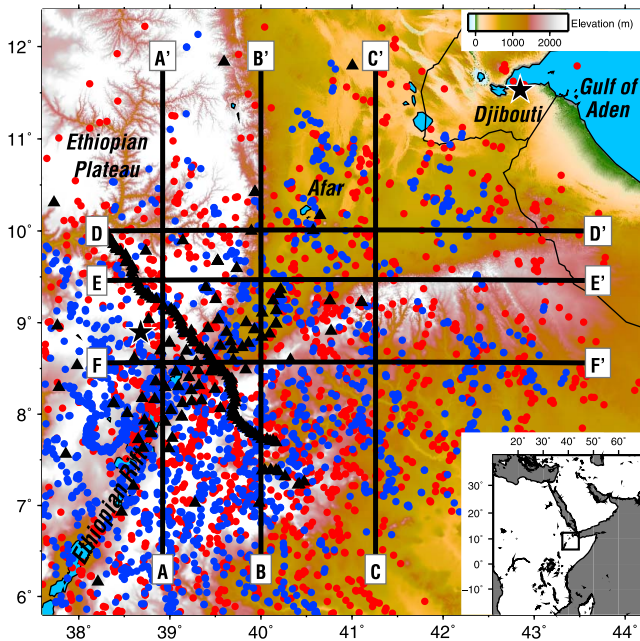


**Figure 1.** Topographical map of the study region with the locations of broadband seismological stations used marked by black triangles (temporary) and stars (permanent, AAE/FURI in Ethiopia and ATD in Djibouti). Calculated piercing point locations at depths of 410 and 660 km are shown as blue and red circles, respectively, using a velocity model including mantle anomalies as defined by *Montelli et al.* [2006]. Labelled black lines show the locations of cross-sectional profiles in Figure 2. The inset indicates the study location in relation to the African continent.

reported no conclusive evidence for the ‘410’ with *P*-to-*S* converted-waves, whereas the ‘660’ is mapped with considerable relief (625–675 km).

### 3. Data and Processing

[8] We utilize teleseismic ( $m_b > 5.8$ ) earthquake data recorded by EAGLE [*Maguire et al.*, 2003] and EBSE [*Nyblade and Langston*, 2002] temporary broadband seismological stations plus permanent stations FURI and ATD (Figure 1 and Figure S1 in the auxiliary material).<sup>1</sup> We use the time domain iterative deconvolution technique of *Ligorria and Ammon* [1999] to calculate RFs that capture *P* to *S* wave conversions from impedance discontinuities within the Earth. We filtered our RFs between 0.033 and 0.25 Hz in order to detect conversions from the MTZ and converted the arrival times of each RF to depth using a model based upon IASP91 [*Kennett and Engdahl*, 1991] but adapted to include regional upper mantle *P* and *S* wave velocity anomalies [*Montelli et al.*, 2006, hereafter M06]. The conversion points were migrated to their correct geometric positions [*Zhu*, 2000] and converted energy binned into voxels and smoothed (according to the size of the Fresnel zone and vertical resolution of the RFs) to produce final migrated images of the MTZ discontinuity depths (we follow a similar data reduction

scheme to *Hetényi et al.* [2009]). The potential vertical resolution of RFs at the considered frequencies and depths is  $\sim 5$  and  $\sim 6$  km at the ‘410’ and ‘660’, whilst the lateral resolution is estimated to be  $\sim 125$  and  $\sim 160$  km, respectively.

### 4. Results

[9] We stack our dataset in its entirety (1923 traces) (Figure S2) to illustrate that both phases are clear with strong amplitudes (mean P410S and P660S are 49.2 and 72.9 seconds after *P*, respectively). The observed phase times are consistent with permanent broadband station studies (P410S =  $49.8 \pm 0.4$  and P660S at  $74.0 \pm 0.2$  seconds at FURI; P410S =  $48.2 \pm 0.2$  and P660S =  $72.6 \pm 0.4$  seconds at ATD) [e.g., *Tauzin et al.*, 2008].

[10] Images through the migrated CCP volume show clear evidence for the ‘410’ and ‘660’ occurring at mean depths of 443 km (range = 434–456 km;  $1\sigma = 3$  km; range =  $\pm 11$  km) and 688 km (665–705 km;  $1\sigma = 8$  km; range =  $\pm 20$  km), respectively (Figure 2). The ‘410’ displays a relatively minor variation in depth when compared to the ‘660’ and is consistently between 440 and 450 km across the majority of the study region. It tends to the deeper end of this range to the SW and appears shallowest in the NE. The ‘660’ is also shallowest in the north-easternmost parts of the study region (reaching 665 km near 500 km along section B–B’) and is deepest in the central and southern parts of the region ( $>700$  km). The north-south deepening is also seen on the succession of west-to-east sections in Figure 2.

[11] The location and depth of the maximum converted energy from both ‘410’ and ‘660’ was manually picked and contoured across the study area. An MTZ thickness map (Figure 3) was made by taking the difference in these contoured surfaces. It is probable that the absolute positions of the ‘410’ and ‘660’ are biased by the global-scale velocity model we use, however, we can assess thickness changes quantitatively because MTZ thickness is derived from P660S–P410S differential travel times that are insensitive to velocity anomalies above the ‘410’.

[12] The MTZ shows important thickness variations ( $\sim 40$  km). It is thinnest in the north-east (225–235 km) and has a thickness of  $\sim 240$  km in the south-west, with a gradient striking approximately NW–SE delineating the edge of a  $\sim 200 \times 200$  km<sup>2</sup> region where the MTZ is thickest (245–265 km). Owing to the greater range of depth variation seen in ‘660’ compared to ‘410’ depths across the area, the MTZ thickness map is similar in appearance to the ‘660’ discontinuity map.

### 5. Discussion

#### 5.1. The 410 Discontinuity

[13] We clearly image the ‘410’, which appears to be depressed by 30–40 km beneath Afar, the MER and both rift flanks. The absolute position of the ‘410’ is primarily governed by the upper mantle velocity model and the local temperature [e.g., *Helffrich*, 2000] (Figure S3).

[14] No part of the ‘410’ is observed at 410 km depth, even though M06 contains upper mantle velocity anomalies (typically  $\delta V_P = -1.8\%$  and  $\delta V_S = -3.8\%$  and similar to other absolute regional velocity models, e.g.,  $\delta V_S = -2.4\%$  [*Ritsema et al.*, 1999]) throughout the study area. We note that fixing the ‘410’ to a mean depth of 410 km requires a

<sup>1</sup>Auxiliary materials are available in the HTML. doi:10.1029/2011GL047575.

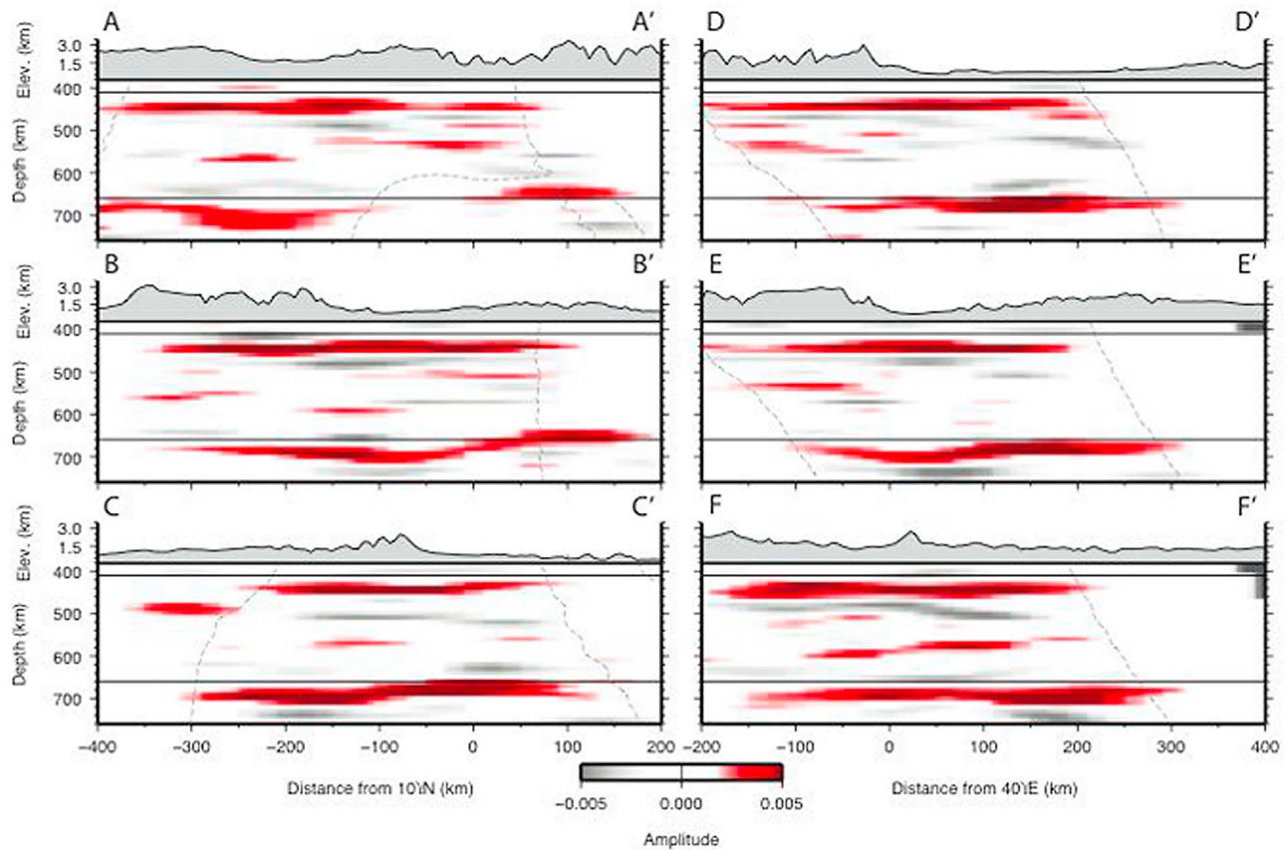


**Figure 2.** Representative cross-sections through the migrated volume using the M06 velocity model (i.e., including mantle anomalies as defined by *Montelli et al.* [2006], compare to Figure S5 to view the effects of the velocity anomalies) that correspond to the profiles marked on Figure 1. The topography along each of these profiles is also shown. Dotted lines mark the extent of well-resolved parts of the volume, as defined by 10% of the maximum hit count.

model containing velocity anomalies a factor of  $\sim 2$  larger than M06 (Figure S3).

[15] Assuming that the M06 velocity model is a correct representation of the upper mantle, we require a  $\sim 250$  °C hot anomaly that pervades the entire study region to explain the ‘410’ position (Clapeyron slope of  $2.9 \text{ MPa K}^{-1}$  [*Bina and Helffrich*, 1994]). An elevated temperature is coherent with the geodynamic context and tomographic results [e.g., *Benoit et al.*, 2006].

[16] We attribute the relatively minor changes in ‘410’ depth across the region to either long-wavelength ( $\geq 200$  km) lateral variations in temperature, or upper mantle velocity heterogeneities that are unaccounted for by the M06 model.

## 5.2. The 660 Discontinuity and MTZ Thickness

[17] The ‘660’ varies in depth from 665 to 705 km within the study region and we resolve a NW-SE striking gradient between the shallowest and deepest region beneath southern

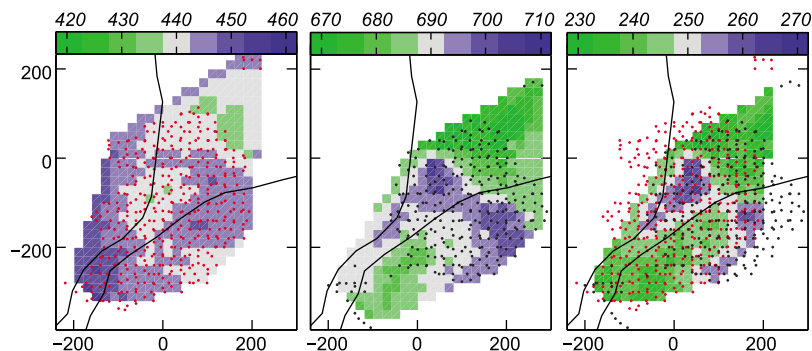


**Figure 3.** Maps of picked depth to 410 and 660 discontinuities and mantle transition zone thickness (TZT) (km). The nominal extent of the Ethiopian rift is shown with black lines. Pick locations for the 410 and 660 discontinuities are shown as red and black dots, respectively, and the X-Y scale is in kilometers relative to  $40^\circ\text{E}$ ,  $10^\circ\text{N}$ .

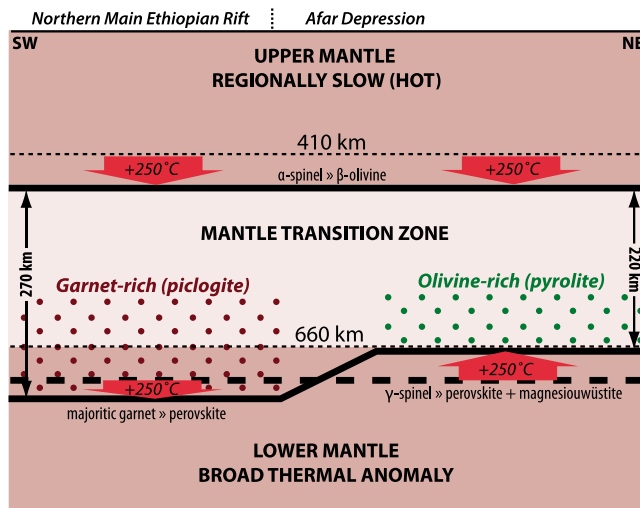


**Figure 4.** A conceptual sketch of our favored explanation for the MTZ structure beneath Ethiopia.

Afar. The MTZ thickness is similar to the ‘660’ topography due to the relatively smaller topography of the ‘410’ and varies from  $>260$  km beneath the NMER to  $<230$  km beneath Afar.

[18] We consider the following possible contributors that dictate the position of the ‘660’ and thus the lateral changes in MTZ thickness: i) the velocity structure within the MTZ; ii) horizontal temperature gradients at the base of the MTZ that affect the depth of the olivine-dominant (pyrolite model) phase transition; iii) a higher ambient temperature of the MTZ that favors the garnet-dominant (piclogite model) phase transition; and iv) compositional heterogeneities within the MTZ.

### 5.2.1. Velocity Structure Within the MTZ

[19] Introducing a horizontal slow-to-fast velocity gradient in the MTZ would produce a thinning in the same direction, but the magnitude of such an anomaly would need to be  $\delta V_P > 5\%$  and  $\delta V_S > 10\%$  within a horizontal distance of  $<100$  km to match the observations. A local tomography study by Chang and Van der Lee [2011] shows that  $S$  wave velocity anomalies within the MTZ are typically  $<1\%$  (although it should be noted that tomographic methods typically underestimate amplitudes of mantle seismic anomalies and suppress steep lateral gradients).

[20] Some regional models predict a slow upper mantle anomaly pervading into the MTZ (e.g., M06 has mean  $\delta V_P = -1.25$  and  $\delta V_S = -2.50\%$  within the MTZ), but these models do not possess the required resolution to image a short-wavelength velocity gradient within this anomaly. It is also highly unlikely that velocity gradients larger than those imaged in the upper mantle [e.g., Benoit et al., 2006; Bastow et al., 2008; Chang and Van der Lee, 2011] are present within the Ethiopian MTZ. We therefore conclude that the effects of lateral velocity changes within the MTZ alone cannot explain our findings.

### 5.2.2. Lateral Temperature Changes

[21] A temperature change of  $>250$  °C within a horizontal distance of  $<200$  km would be required to vary the olivine-dominant 660’ phase transition by 35–40 km in depth (assuming a Clapeyron slope of  $-1.9$  MPa  $K^{-1}$  [Bina and

Helfrich, 1994]). Since there is little evidence for a large velocity gradient near the ‘660’ [e.g., Chang and Van der Lee, 2011] and, assuming that  $S$  wave tomography is an indicator of temperature [e.g., Karato, 1993], we do not expect that the required temperature gradient is present beneath Ethiopia.

[22] Combining the effects of the temperature and velocity anomalies described above *does not* help to explain the observed ‘660’ depth variation as they have opposite effects: a narrowing of the MTZ would require a change towards a faster but hotter anomaly; whereas a thickening of the MTZ would require a change towards slower but colder anomaly. This scenario is therefore unlikely.

### 5.2.3. Majorite to Ca-Perovskite Transition

[23] Our ‘660’ RF amplitudes could correspond to the majorite  $\rightarrow$  Ca-perovskite transition rather than to the phase change of olivine [Deuss, 2007]. The commonly-used pyrolite mantle model contains 40 % majorite that may become the dominant phase transition at high temperature [Ringwood, 1975; Vacher et al., 1998; Weidner and Wang, 2000; Hirose, 2002] (Figure S4). This is a plausible scenario because a plume rising from the lower mantle (as imaged beneath Ethiopia by global tomography) represents a thermal anomaly that could raise the temperature near the base of the MTZ to  $>1800$  °C. Although the higher temperatures are more favorable for the garnet-dominant phase change to be present [e.g., Hirose, 2002], the relatively small Clapeyron-slope ( $+1.3$  MPa  $K^{-1}$  [Bina and Helfrich, 1994]) implies that a temperature anomaly of  $>600$  °C is required to change the depth of the ‘660’ by the  $>30$  km we observe. Therefore, even if the ambient temperature is such that the garnet transition is dominant, temperature alone cannot explain the observed depth variations.

[24] However, combining a garnet-dominated composition with both high temperature and slow velocity anomalies *does* help to explain the thickest parts of the MTZ. The positive Clapeyron-slope of the majorite  $\rightarrow$  Ca-perovskite phase transition means narrowing of the MTZ (an uplift of the ‘660’) is here coherent with faster MTZ velocity and *cooler* temperature and a thickening is associated to changes towards slower and hotter values. This combination of compositional effects together with potential temperature and velocity trends is our preferred model. It is similar to that proposed to explain a regionally-deepened ‘660’ (at  $\sim 680$  km) beneath Kenya and Tanzania [Huerta et al., 2009].

### 5.2.4. Compositional Heterogeneity

[25] Whilst we have explained the thickest observed MTZ, in order to explain a 35–40 km change between neighboring thinned and thickened MTZ regions that are probably at similar temperatures, we require a compositional change in the lower parts of the MTZ. In other words, we require horizontal changes in the MTZ composition between more piclogitic [Anderson and Bass, 1986] and more pyrolitic [Ringwood, 1975] parts (Figure S4). Thick MTZ regions occur where the composition has greater amounts of garnet relative to olivine and a greater proportion of  $Al_2O_3$  [e.g., Vacher et al., 1998] (Figure 4) whereas thinned MTZ regions are dominated by olivine and the negative Clapeyron slope at the ‘660’. Such a compositional change would take place in a mantle with a high ambient temperature and would cause changes in MTZ thickness.

[26] Compositional changes at the base of the MTZ are normally attributed to foundering of subducted oceanic or

detached subcontinental lithosphere that sank to the base of the MTZ [e.g., Green *et al.*, 2010]. However, compressional tectonics last occurred in Ethiopia ~550 Myr ago [Stern, 1994], perhaps suggesting that we have imaged a long-lived compositional heterogeneity that is elucidated by elevated mantle temperatures. The origin and persistence of chemical heterogeneities in the MTZ are the subjects of ongoing investigations using thermo-chemical models [e.g., Cammarano *et al.*, 2003].

## 6. Conclusions

[27] We use receiver functions to map the mantle transition zone structure beneath Ethiopia including Afar by clearly imaging the 410 and 660 discontinuities.

[28] The '410' is flat and regionally depressed by 30–40 km, most likely caused by a combination of slow upper mantle velocities and high temperatures.

[29] The '660' has depth changes (665–705 km) over short distances (<200 km), resulting in a overall thinned MTZ (mean thickness = 244 km) that is locally thickened to over 260 km.

[30] Geologically plausible temperature and velocity changes both individually and combined are insufficient to explain the '660' depth changes and hence MTZ thickness variations.

[31] Our preferred model has two adjacent chemical compositions with contrasting amounts of garnet at the base of the MTZ. In the presence of a hot lower mantle, a majorite → Ca-perovskite phase transition (deeper '660') would be favored in a piclogitic MTZ, whereas a ringwoodite ( $\gamma$ -olivine) to Mg-perovskite + magnesiowustite (shallower '660') phase transition would occur in a piclogitic MTZ, resulting in the abrupt MTZ thickness changes we observe.

[32] The requirement of high ambient MTZ temperature provides evidence that the Ethiopian upper mantle low velocity anomaly is linked to the lower mantle African Superplume across the MTZ.

[33] **Acknowledgments.** Valuable discussions with Rosie Fletcher, Derek Keir, Geoff Lloyd, Dan Morgan, Jon Mound, Sebastian Rost and Graham Stuart and velocity model help from Sheona Masterton and Ian Bastow are acknowledged. Tim Wright is thanked for providing computing resources. Adobe Illustrator and GMT [Wessel and Smith, 1995] were used during all figure preparation.

[34] The Editor thanks the two anonymous reviewers for their assistance in evaluating this paper.

## References

- Anderson, D. L., and J. Bass (1986), Transition region of the Earth's upper mantle, *Nature*, **320**, 321–328.
- Bastow, I. D., A. A. Nyblade, G. W. Stuart, T. O. Rooney, and M. H. Benoit (2008), Upper mantle seismic structure beneath the Ethiopian hot spot: Rifting at the edge of the African low-velocity anomaly, *Geochem. Geophys. Geosyst.*, **9**, Q12022, doi:10.1029/2008GC002107.
- Benoit, M. H., A. A. Nyblade, T. J. Owens, and G. Stuart (2006), Mantle transition zone structure and upper mantle S velocity variations beneath Ethiopia: Evidence for a broad, deep-seated thermal anomaly, *Geochem. Geophys. Geosyst.*, **7**, Q11013, doi:10.1029/2006GC001398.
- Bina, C. R., and G. Helffrich (1994), Phase transition Clapeyron slopes and transition zone seismic discontinuity topography, *J. Geophys. Res.*, **99**, 15,853–15,860, doi:10.1029/94JB00462.
- Cammarano, F., S. Goes, P. Vacher, and D. Giardini (2003), Inferring upper-mantle temperatures from seismic velocities, *Phys. Earth Planet. Inter.*, **138**, 197–222.
- Chang, S.-J., and S. Van der Lee (2011), Mantle plumes and associated flow beneath Arabia and East Africa, *Earth Planet. Sci. Lett.*, **302**, 448–454, doi:10.1016/j.epsl.2010.12.050.
- Cornwell, D. G., P. K. H. Maguire, R. W. England, and G. W. Stuart (2010), Imaging detailed crustal structure and magmatic intrusion across the Ethiopian Rift using a dense linear broadband array, *Geochem. Geophys. Geosyst.*, **11**, Q0AB03, doi:10.1029/2009GC002637.
- Deuss, A. (2007), Seismic observations of transition zone discontinuities beneath hotspot locations, in *Plates, Plumes, and Planetary Processes*, edited by G. Foulger and D. Jurdy, *Spec. Pap. Geol. Soc. Am.*, **430**, 121–136.
- Dugda, M. T., A. A. Nyblade, and J. Julia (2007), Thin lithosphere beneath the Ethiopian plateau revealed by a joint inversion of Rayleigh wave group velocities and receiver functions, *J. Geophys. Res.*, **112**, B08305, doi:10.1029/2006JB004918.
- Ebinger, C. J., and M. Casey (2001), Continental breakup in magmatic provinces: An Ethiopian example, *Geology*, **29**, 527–530.
- Green, H. W., W.-P. Chen, and M. R. Brudzinski (2010), Seismic evidence of negligible water carried below 400-km depth in subducting lithosphere, *Nature*, **467**, 828–831, doi:10.1038/nature09401.
- Helffrich, G. (2000), Topography of the transition zone seismic discontinuities, *Rev. Geophys.*, **38**, 141–158.
- Hetényi, G., G. W. Stuart, G. A. Houseman, F. Horváth, E. Hegedus, and E. Brückl (2009), Anomalously deep mantle transition zone below Central Europe: Evidence of lithospheric instability, *Geophys. Res. Lett.*, **36**, L21307, doi:10.1029/2009GL040171.
- Hirose, K. (2002), Phase transitions in pyrolitic mantle around 670-km depth: Implications for upwelling of plumes from the lower mantle, *J. Geophys. Res.*, **107**(B4), 2078, doi:10.1029/2001JB000597.
- Huerta, A. D., A. A. Nyblade, and A. M. Reusch (2009), Mantle transition zone structure beneath Kenya and Tanzania: More evidence for a deep-seated thermal upwelling in the mantle, *Geophys. J. Int.*, **177**, 1249–1255, doi:10.1111/j.1365-246X.2009.04092.x.
- Karato, S. (1993), Importance of anelasticity in the interpretation of seismic tomography, *Geophys. Res. Lett.*, **20**, 1623–1626.
- Kennett, B., and E. R. Engdahl (1991), Traveltimes for global earthquake location and phase identification, *Geophys. J. Int.*, **105**, 429–465.
- Lawrence, J. F., and P. M. Shearer (2006), A global study of transition zone thickness using receiver functions, *J. Geophys. Res.*, **111**, B06307, doi:10.1029/2005JB003973.
- Ligorria, J., and C. J. Ammon (1999), Iterative deconvolution of teleseismic seismograms and receiver function estimation, *Bull. Seismol. Soc. Am.*, **89**, 1395–1400.
- Maguire, P. K. H., et al. (2003), Geophysical project in Ethiopia studies continental breakup, *Eos Trans. AGU*, **84**(35), doi:10.1029/2003EO350002.
- Montelli, R., G. Nolet, F. A. Dahlen, and G. Masters (2006), A catalogue of deep mantle plumes: New results from finite-frequency tomography, *Geochem. Geophys. Geosyst.*, **7**, Q11007, doi:10.1029/2006GC001248.
- Nyblade, A. A., and C. A. Langston (2002), Broadband seismic experiments probe the East African rift, *Eos Trans. AGU*, **83**(37), doi:10.1029/2002EO000296.
- Nyblade, A. A., R. P. Knox, and H. Gurrrola (2000), Mantle transition zone thickness beneath Afar: implications for the origin of the Afar hotspot, *Geophys. J. Int.*, **142**, 615–619.
- Ringwood, A. E. (1975), *Composition and Petrology of the Earth's Mantle*, McGraw-Hill, New York.
- Ritsema, J. H., J. van Heijst, and J. H. Woodhouse (1999), Complex shear wave velocity structure imaged beneath Africa and Iceland, *Science*, **286**, 1925–1928.
- Simmons, N. A., A. M. Forte, and S. P. Grand (2007), Thermochemical structure and dynamics of the African superplume, *Geophys. Res. Lett.*, **34**, L02301, doi:10.1029/2006GL028009.
- Stern, R. J. (1994), Arc assembly and continental collision in the Neoproterozoic east African Orogen: Implication for the consolidation of Gondwanaland, *Annu. Rev. Earth Planet. Sci.*, **22**, 319–351.
- Tauzin, B., E. Debayle, and G. Wittlinger (2008), The mantle transition zone as seen by global Pds phases: No clear evidence for a thin transition zone beneath hotspots, *J. Geophys. Res.*, **113**, B08309, doi:10.1029/2007JB005364.
- Vacher, P., A. Mocquet, and C. Sotin (1998), Computation of seismic profiles from mineral physics: the importance of the non-olivine components for explaining the 660 km depth discontinuity, *Phys. Earth Planet. Inter.*, **106**, 275–298.
- Weidner, D. J., and Y. Wang (2000), Phase transformations: Implications for mantle structure, in *Earth's Deep Interior: Mineral Physics and Tomography from the Atomic to the Global Scale*, *Geophys. Monogr. Ser.*, vol. 117, edited by S. Karato et al., pp. 215–235, AGU, Washington, D. C.

- Wessel, P., and W. H. F. Smith (1995), New version of the generic mapping tools released, *Eos Trans. AGU*, 76, 329.
- Wolfenden, E., C. Ebinger, G. Yirgu, A. Deino, and D. Ayalew (2004), Evolution of the northern Main Ethiopian rift: Birth of a triple junction, *Earth Planet. Sci. Lett.*, 224, 213–228.
- Wright, T. J., C. Ebinger, J. Biggs, A. Ayele, G. Yirgu, D. Keir, and A. Stork (2006), Magma-maintained rift segmentation at continental rapture in the 2005 Afar dyking episode, *Nature*, 442, 291–294, doi:10.1038/nature04978.
- Zhu, L. P. (2000), Crustal structure across the San Andreas Fault, Southern California from teleseismic converted waves, *Earth Planet. Sci. Lett.*, 179, 183–190, doi:10.1016/S0012-821X(00)00101-1.
- 
- T. D. Blanchard and D. G. Cornwell, School of Earth and Environment, University of Leeds, Woodhouse Lane, Leeds LS2 9JT, UK. (t.blanchard@see.leeds.ac.uk; d.cornwell@see.leeds.ac.uk)
- G. Hetényi, Institut für Geochemie und Petrologie, ETH Zurich, NW E 82, Clausiusstrasse 25, CH-8092 Zürich, Switzerland. (gyorgy.hetenyi@erdw.ethz.ch)